UC Berkeley

UC Berkeley Previously Published Works

Title

Global evidence for the acclimation of ecosystem photosynthesis to light

Permalink

https://escholarship.org/uc/item/9vk6r914

Journal

Nature Ecology & Evolution, 4(10)

ISSN

2397-334X

Authors

Luo, Xiangzhong Keenan, Trevor F

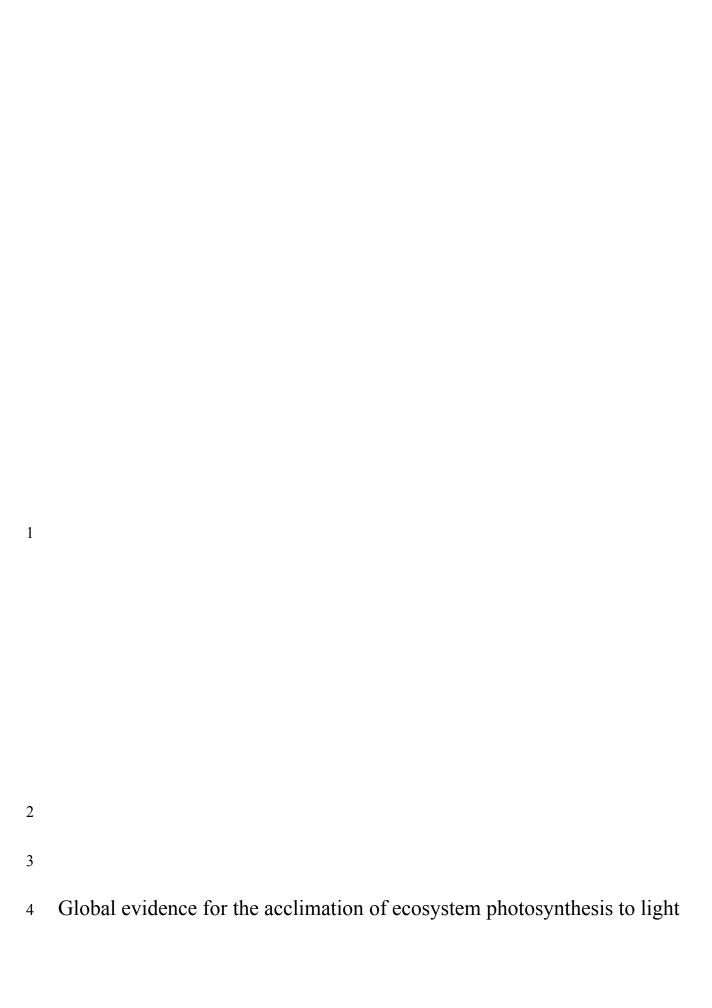
Publication Date

2020-10-01

DOI

10.1038/s41559-020-1258-7

Peer reviewed



Xiangzhong Luo ^{1,2}, Trevor F. Keenan ^{1,2} ¹ Climate and Ecosystem Sciences Division, Lawrence Berkeley National Laboratory ² Department of Environmental Science, Policy and Management, University of California, Berkelev Correspondence: X.L. xzluo@lbl.gov T.F.K. trevorkeenan@berkeley.edu

Abstract

Photosynthesis responds quickly to changes in light, increasing with incoming photosynthetic photon flux density (PPFD) until leaves become light saturated. This instantaneous response to PPFD, which is widely studied and incorporated into models of photosynthesis, is overlaid on non-instantaneous photosynthetic changes resulting from the acclimation of plants to average PPFD over intermediate timescales of a week to months (\overline{PPFD}). Such photosynthetic light acclimation is not typically incorporated into models, due to the lack of observational constraints. Here, we use eddy covariance observations from globally distributed and automated sensor networks, along with photosynthesis estimates from 9 terrestrial biosphere models (TBMs) to quantify and assess photosynthetic acclimation to light in natural environments. In addition, we use recent theoretical developments to incorporate light acclimation in a TBM. Our results show widespread light acclimation of ecosystem photosynthesis. On average, a 1 μ mol m⁻² s⁻¹ increase

in \overline{PPFD}_{10} (10-day average PPFD) leads to a 0.031 \pm 0.013 μ mol C m⁻² s⁻¹ increase in maximum photosynthetic assimilation rate (A_{max}), with croplands having a stronger acclimation rate than grasslands and forests. Our analysis shows that the TBMs examined either neglect or substantially underestimate light acclimation. By updating a TBM to include photosynthetic acclimation, successfully reproducing the \overline{PPFD}_{10} -A_{max} relationship, we provide a robust method for the incorporation of photosynthetic light acclimation in future models.

Main

Global photosynthesis is the largest carbon flux in the global carbon cycle 1 , removing CO $_2$ from the atmosphere and thus contributing to climate change mitigation. The amount of carbon assimilated by photosynthesis is dependent on the short- and long-term responses of vegetation to a range of climate factors, in particular incoming solar irradiance, about half of which is photosynthetically active photons 2 . The intensity of incoming photosynthetic active photons is described by photosynthetic photon flux density (PPFD; unit: μ mol photon m $^{-2}$ s $^{-1}$). PPFD is utilized by leaves in a fast biochemical process that converts photonic energy into biochemical energy to drive the Calvin-Benson cycle and ultimately fix CO $_2$ into starches and sugars that are used to maintain metabolism and grow biomass 3 . The relationship between the instantaneous rate of photosynthesis (A) and PPFD has been well documented using light response curves, in which A generally increases with PPFD and plateaus at maximum A (A_{max}) when leaves become light saturated 4 .

The well documented light response curves, and the understanding of leaf biochemical processes generated from them, form the basis of many terrestrial biosphere models (TBMs), the principle

tools used to estimate the terrestrial carbon cycle 5 . In such models, however, PPFD only influences instantaneous rates of photosynthetic carbon assimilation. This approach is at odds with results from field experiments, which show that, over intermediate timescales of a week to months, plants also respond to increasing PPFD by increasing A_{max} $^{6-10}$. Experimental observations consistently show that leaves exposed to higher average levels of PPFD over intermediate timescales (\overline{PPFD}) tend to have larger A_{max} . For example, leaf-level A_{max} can increase from less than 5 μ mol C m⁻² s⁻¹ to more than 15 μ mol C m⁻² s⁻¹ while autumn \overline{PPFD} increases from approximately 50 μ mol photon m⁻² s⁻¹ to 600 μ mol photon m⁻² s⁻¹. This strategic adjustment to \overline{PPFD} improves plant light-use efficiency, a process known as photosynthetic light acclimation, to further increase the magnitude of instantaneous A.

limited species in controlled experiments, providing an incomplete picture of the existence, degree and pattern of photosynthetic light acclimation in natural ecosystems. Additionally, many studies have found that the within-canopy gradient of leaf-level photosynthetic capacity is optimized to follow the within canopy light profile ^{11,12}, indicating that leaf-level light acclimation underlies the ecosystem-scale photosynthetic activity. However, the connection between leaf and ecosystem light acclimation has remained elusive, as direct evidence of ecosystem-scale light acclimation is lacking, as is an effective method to simulate acclimation. Hence, photosynthetic light acclimation is ignored in state-of-the-art TBMs ¹³. Globally distributed observations of ecosystem carbon fluxes based on the eddy-covariance technique ^{14,15}, and the resulting estimates of ecosystem gross primary productivity ¹⁶, offer a unique opportunity to examine the degree of photosynthetic light acclimation in natural ecosystems. In tandem,

Historically, studies have investigated photosynthetic light acclimation at the leaf scale and for

recent theoretical developments, in particular the coordination hypothesis, which suggests that plant photosynthesis acclimates at intermediate timescales of weeks to months ^{17–21}, provide a potential approach to incorporate the process of photosynthetic light acclimation into TBMs.

Here, we use globally distributed eddy covariance measurements from more than a hundred sites to examine ecosystem scale photosynthetic light acclimation. We estimate ecosystem A_{max} using a light response curve approach 16 across all sites, and characterize the ecosystem light acclimation rate (γ_A) as the sensitivity of A_{max} to \overline{PPFD}_{10} (i.e. 10-day average PPFD). The objectives of this study are to examine whether and to what degree ecosystem photosynthetic light acclimation (i.e. positive γ_A) occurs, to understand the distribution of γ_A along environmental and ecological gradients, to evaluate TBMs using γ_A inferred from observations, and to develop and test an approach to incorporate photosynthetic light acclimation into TBMs.

Results and Discussion

We derived ecosystem A_{max} from half-hourly net ecosystem carbon exchange measured at eddy covariance sites covering a wide range of variation in A_{max} and environmental factors. Multiple environmental factors co-vary with PPFD on intermediate timescales, in particular daytime air temperature (T_{air}) and vegetation foliage densities (indicated by fraction of absorbed photosynthetic active ration; fAPAR; unitless). In order to remove the influence of extraneous environmental variability, we grouped the derived A_{max} and observed \overline{PPFD}_{10} into bins by their corresponding fAPAR and T_{air} (see Methods) and then quantified γ_A within each bin (Fig.1). In addition to removing extraneous influences on the derived photosynthetic light acclimation, this also allowed us to examine light acclimation across environmental gradients. We detected

acclimation under natural conditions (Fig. 1a). 59.8% of those positive PPFD₁₀-A_{max} correlations were statistically significant (p < 0.1; 48.1% for p < 0.05). Our analysis found an average γ_A of 0.031 ± 0.013 mol mol⁻¹ (µmol C m⁻² s⁻¹ per µmol photon m⁻² s⁻¹; mean \pm s.d.) for the significant acclimation cases (p < 0.1). Changes in the length of the time windows we used to detect light acclimation did not affect our results (Extended Data Fig. 1). We used a linear regression of Amax to \overline{PPFD}_{10} to derive γ_A (Fig. 1b) as it was commonly adopted by previous leaf-level experiments ^{6,9}, though we acknowledge cases where A_{max} responded to \overline{PPFD} non-linearly ^{8,10}. The ecosystem γ_A (0.031 \pm 0.013 mol mol⁻¹) we derived from the eddy covariance data was comparable to the leaf-level γ_A (0.027 \pm 0.016 mol mol⁻¹) we collated from previous studies (Fig. 1c; Supplementary Table 1). It should be noted that ecosystem γ_A is the slope of the regression of canopy A_{max} (µmol C m⁻² ground surface area s⁻¹) to \overline{PPFD}_{10} (µmol photon m⁻² ground surface area s⁻¹), while leaf γ_A is the slope of the regression of leaf A_{max} (µmol C m⁻² leaf area s⁻¹) to \overline{PPFD}_{10} (µmol photon m⁻² ground surface area s⁻¹), meaning that ecosystem γ_A is equal to the sum of γ_A of all leaves in a canopy divided by total leaf area (a.k.a. the average leaf γ_A). The ecosystem γ_A we derived is therefore comparable to published leaf-level γ_A (Fig. 1c). We note that using an A_{max} standardized to a PPFD of 2000 μ mol m⁻² s⁻¹ resulted in a somewhat lower γ_A of 0.025 ± 0.012 mol mol⁻¹ (Extended Data Fig. 2). Although we show light acclimation is related to light intensity (i.e. \overline{PPFD}_{10}), some studies

positive γ_A in 85% of the bins studied, suggesting a widespread existence of photosynthetic light

97

98

99

100

101

102

103

104

105

106

107

108

109

110

111

112

113

114

115

116

117

118

119

suggested photoperiod 22 and the total amount of photons 10 received by vegetation can cause changes in A_{max} . We assessed the dependence of A_{max} on photoperiod (the number of daytime hours in a day; unit: hours) and total photons (mol m⁻² day⁻¹) of the same 10-day windows, and

found positive γ_A in more than 80% of the bins in both cases (Extended Data Fig. 3). The patterns of γ_A we derived from the regressions of A_{max} to photoperiod and total photons were very similar to what we obtained when using \overline{PPFD}_{10} (Fig. 1a), potentially caused by the strong correlations between three light metrics. In this study, we used \overline{PPFD}_{10} as the primary predictor in order to compare with theoretical acclimation predictions of the response of A_{max} to light intensity.

We further examined several potential drivers to explain the changes in ecosystem γ_A . First, we found that ecosystem γ_A (the average γ_A of bins with significant (p < 0.1) light acclimation) was relatively insensitive to fAPAR between 0.4 to 0.6, as γ_A stabilized at 0.028 ± 0.011 mol mol⁻¹ (Fig. 2a). However, for dense canopies where fAPAR > 0.6, γ_A significantly increased with fAPAR to 0.041 ± 0.015 mol mol⁻¹ (p < 0.05; Fig. 2a; Extended Data Fig. 1). Considering that ecosystem γ_A indicates the average leaf γ_A within a canopy, and that shaded leaves constitute an increasingly larger portion of a canopy as fAPAR increases (Extended Data Fig. 4)²³, our results indicate that shaded leaves acclimate to light faster than sunlit leaves. This suggests a nonlinear and gradually saturating response of A_{max} to \overline{PPFD} , which has been proposed by a meta-analysis though some studies suggested otherwise 6.8. Meanwhile, the changes in fAPAR did not influence the detectability of light acclimation (i.e. the ratio of the number of the bins where $\gamma_A > 0$ and p < 0.1 to the total number of bins) using our method, as the detectability stabilized at 60%.

We found that the detectability of light acclimation changed as a function of T_{air} , with detectability declining from almost 100% to 0% when T_{air} either increased or decreased from

detectability of acclimation at low temperature could potentially be caused by photoinhibition, a light-induced process that damages photosystem II and downregulates A_{max} ²⁴ and consequently influences γ_A . Several studies have found that the effect of photoinhibition is particular evident at low temperature ^{25–27}, though there are conflicting reports over the temperature dependence of photoinhibition ²⁸. In addition, we found that the decreased detectability of light acclimation under high temperature was related to the effect of vapor pressure deficit (VPD) on stomatal conductance (Fig. 2d). Stomatal aperture is inversely related to VPD ^{29,30}, and stomatal closure could reduce A_{max} and hence influence γ_A . Note however that our data pre-filtering criteria removed most periods with moderate to high VPD (see Methods section 3), in order to minimize the VPD effect on γ_A . For those bins with significant (p < 0.1) light acclimation, γ_A was 0.033 \pm $0.017 \text{ mol mol}^{-1}$ for $T_{air} < 10 \,^{\circ}\text{C}$, $0.027 \pm 0.010 \,^{\circ}\text{mol mol}^{-1}$ for T_{air} between 10 $^{\circ}\text{C}$ and 20 $^{\circ}\text{C}$, and 0.039 ± 0.013 mol mol⁻¹ for T_{air} > 20 °C. (Fig. 2b; Extended Data Fig. 1). The significantly higher γ_A (t-test, p < 0.05) under warmer conditions is consistent with some previous reports^{31,32}, though a lack of experimental observations on the temperature dependence of light acclimation precludes a mechanistic explanation. We also noted that the higher percentage of data pairs from cropland and broadleaf forests (Extended Data Fig. 5), which had a higher acclimation rate (Fig. 2c), might explain the higher γ_A we found under warm conditions. γ_A varied by plant functional type (PFT) (Fig. 2c; Extended Data Fig. 6), with croplands (CRO)

around 10 °C to the higher or lower end of the temperature range (Fig. 2b). The decreased

143

144

145

146

147

148

149

150

151

152

153

154

155

156

157

158

159

160

161

γ_A varied by plant functional type (PFT) (Fig. 2c; Extended Data Fig. 6), with croplands (CRO)
 having the largest acclimation rate around 0.073 ± 0.117 mol mol⁻¹, followed by evergreen
 broadleaf forests (EBF; 0.052 ± 0.058 mol mol⁻¹), deciduous broadleaf forests (DBF; 0.049 ±
 0.077 mol mol⁻¹), grasslands (GRA; 0.045 ± 0.042 mol mol⁻¹), mixed forests (MF; 0.034 ± 0.059

mol mol⁻¹) and evergreen needleleaf forests (ENF; 0.032 ± 0.043 mol mol⁻¹). γ_A from CRO was significantly larger than γ_A of the others (t-test, p < 0.05). This variation in γ_A reflects a difference in the photosynthetic plasticity between PFTs, with some studies attributing the interspecies variations in photosynthetic plasticity to successional stages 33 and nutrient use strategies 34 . The inter-PFT variation in γ_A is potentially related to nitrogen use efficiency (NUE), which could influence A_{max} 35 . The rank ordering of γ_A we observed for each PFT (CRO > DBF = EBF > ENF) (Fig. 2c), was similar to the rank ordering of NUE reported based on the global TRY plant trait database 36 . We note that some bins had negative γ_A , though most of the negative γ_A were not statistically significant (Extended Data Fig. 6). Uncertainties in γ_A , as well as the occurrences of negative γ_A , can be caused by some light properties (i.e. spectral quality 37 and light fluctuations 38,39) and biological factors (i.e. leaf age 40) that are known to impact light acclimation but not considered here. We also note that most negative γ_A values corresponded to bins with few data pairs (i.e. only 6-60 pairs per bin) available to constrain the A_{max} - \overline{PPFD}_{10} relationship (Extended Data Fig. 5 and 7).

We further tested nine TBMs (Supplementary Table 3) to assess the degree of γ_A in their simulations (Fig. 3a). We found that none of the models captured the observed distribution of γ_A , with five models showing positive but underestimated γ_A (BEPS 0.011 \pm 0.021 mol mol⁻¹; CN-CLASS 0.007 \pm 0.030 mol mol⁻¹; ECOSYS 0.023 \pm 0.025 mol mol⁻¹; SiBCASA 0.006 \pm 0.017 mol mol⁻¹; SSiB2 0.004 \pm 0.010 mol mol⁻¹) and four models showing zero or negative mean γ_A (Can-IBIS -0.011 \pm 0.008 mol mol⁻¹; ORCHIDEE -0.010 \pm 0.016 mol mol⁻¹; SiB -0.007 \pm 0.016 mol mol⁻¹; TECO -0.029 \pm 0.021 mol mol⁻¹). Non-zero γ_A in models that do not explicitly account for acclimation can potentially arise due to a prescribed variation in the maximum

carboxylation rate (Vc_{max}), which influences simulated A_{max} under light saturation conditions ³⁶. However, Vc_{max} variation in the examined TBMs is dependent on either biomass allocation ⁴¹, or soil nutrient limitation and optimized water use ⁴², or a simple scaling factor ⁴³, rather than the direct acclimation of A_{max} to \overline{PPFD}_{10} . These empirical methods are often generalized from local studies and prone to estimating biased γ_A when extrapolated to large scales (Fig. 3a), highlighting a need to explicitly consider the \overline{PPFD}_{10} - A_{max} relationship in TBMs.

Recent theoretical advances provide an opportunity to implement photosynthetic light acclimation from the first principles of photosynthesis. Here, we tested an approach that predicts the responses of Vc_{max} to multiple environmental factors from first principles ¹⁹, and which can be used to predict the acclimation of A_{max} to light. The model was developed based on the coordination hypothesis which suggests that the light and dark reactions of photosynthesis are coordinated to optimize light use efficiency ^{17–21} (see Methods). We incorporated this optimality model in one of the TBMs investigated, BEPS ^{44,45}, and found that γ_A significantly improved (*t*-test, p < 0.05) from 0.011 \pm 0.021 mol mol⁻¹ in the original BEPS to 0.023 \pm 0.014 mol mol⁻¹ in the updated BEPS (BEPS-opt) (Fig. 3b). The improvement in γ_A resulted in a 5.2% increase in the intra-annual variation in estimated gross primary productivity (GPP) and a 28.9% increase (*t*-test, p < 0.05) in the inter-annual variation in estimated GPP, which were closer to the variations in GPP we derived from eddy covariance observations (Fig. 3c, d).

Photosynthetic light acclimation is a key feature of plants that leads to spatial and temporal changes in global photosynthesis and ecosystem carbon uptake. In this study, we analyzed a database of eddy covariance observations and found widespread photosynthetic light acclimation.

The global average acclimation rate detected was $0.031 \pm 0.013 \text{ mol mol}^{-1}$ (p < 0.1), which is comparable to the previously reported leaf-level acclimation rate. The acclimation rate of croplands was observed to be stronger than that of forests and grasslands. The observed light acclimation was independent of changes in canopy leaf area for sparse canopies but increase with foliage amount for dense canopies, potentially suggesting shaded leaves acclimate faster to light than sunlit leaves. Low temperature reduced the detectability of light acclimation potentially due to photoinhibition, and high temperature did so by increasing VPD and the resulting stomatal closure. Nine state-of-the-art TBMs we tested failed to accurately reproduce the magnitude of light acclimation we observed. By incorporating a recently developed optimality model in a TBM, we constrained the associated uncertainty and successfully reproduced the magnitude of observed light acclimation. Together, these results suggest that the long-observed acclimation of photosynthesis to light at the leaf scale is also prevalent at the ecosystem scale, and provide an effective approach for its incorporation into land surface models.

Methods

1. Derivation of A_{max} from eddy covariance measurements

We used eddy covariance observations of carbon exchange between ecosystems and the atmosphere provided in the standard FLUXNET2015 Tier 1 dataset ⁴⁶. It provides half-hourly and hourly net carbon flux (F_c) and their concurrent meteorological records for 166 sites from different regional networks (Supplementary Table 2). We used gap-filled meteorological records including incoming solar radiation (SW IN F), air temperature (TA F) and vapor pressure

- 234 deficit (VPD_F) to derive the seasonal varying A_{max} of eddy covariance sites from non-gap-filled
- F_c measurements.
- F_c is the balance of CO₂ taken up by photosynthesis and released by respiration. In the process of
- partitioning F_c into an ecosystem photosynthesis and respiration term using the daytime
- partitioning method 16,47 , a key step is to fit F_c with a light response curve (LRC):

$$239 F_c = \frac{\alpha \beta R_g}{\alpha R_g + \beta} + \gamma (1)$$

- where α (µmol J⁻¹) is the canopy-scale quantum yield, β is the maximum rate of CO₂ uptake of
- the canopy under saturating light levels (μ mol photon m⁻² s⁻¹), which is equivalent to A_{max} . R_g is
- 242 the global radiation and γ is the ecosystem respiration term. The impact of VPD on β is
- considered by requiring that β decreases exponentially with the increase of VPD when VPD
- 244 exceeds a threshold (VPD_0).

245
$$\beta = \begin{cases} \beta_0 \exp(-k(\text{VPD} - \text{VPD}_0)), \text{VPD} > \text{VPD}_0 \\ \beta_0, \text{VPD} \le \text{VPD}_0 \end{cases}$$
 (2)

- where β_0 and k are fitted parameters and VPD₀ is 10 hPa ⁴⁷.
- To account for the seasonal variation in A_{max} , we applied the equations above to a short time
- 248 window (2-14 days) of F_c depending on the availability of flux measurements (Extended Data
- Fig. 8), and assumed every day in the same time window has the same daily A_{max} . We retrieved
- 250 the daily A_{max} of these 166 sites by implementing equations (1) and (2) using the REddyProc R
- package (https://github.com/bgctw/REddyProc), and we found the majority of the fitted LRCs
- were robust for A_{max} retrievals (Extended Data Fig. 9).
- After obtaining daily A_{max} , we calculated the average A_{max} for every adjacent and non-
- overlapped 10-day window for each site. \overline{PPFD}_{10} and T_{air} are the averages of the daytime PPFD

and daytime air temperature within the same 10-day window. fAPAR in each 10-day window was acquired by interpolating the 8-day MODIS fAPAR time series (MOD15A2H) at each site.

257

258

259

260

261

262

263

264

265

266

267

268

269

270

271

272

273

274

275

276

277

255

256

2. Derivation of A_{max} from the estimates of terrestrial biosphere models

The North America Carbon Program (NACP) site-level interim synthesis is a model-data comparison aimed at discerning the impact of different model structures on carbon flux estimates. The program data repository (https://daac.ornl.gov/NACP/) provides access to the estimates of Gross Primary Productivity (GPP) from 22 TBMs and their corresponding meteorological records at 41 eddy covariance sites located in US and Canada (Supplementary Table 4) 48. To obtain the A_{max} of these sites from the TBMs estimates, we used hourly estimates of GPP 49 along with hourly meteorological records (PPFD, air temperature, VPD) and MODIS fAPAR obtained from the NACP repository ⁵⁰, and fitted the LRC to these hourly GPP and meteorological variables (Equation 1). Since we used GPP as the F_c term in equation (1) in this step, the respiration term (γ) was fixed at 0. Because GPP estimates from models are temporally continuous, we applied this LRC to a time window of 10 days directly to get an A_{max} for every 10 days. PPFD₁₀ and T_{air} are the averages of the daytime PPFD and air temperature within the same 10-day window. We retrieved A_{max} from modelled GPP for all 22 TBMs in NACP using equations (1) and (2) (https://github.com/lxzswr/simpleLRC). However, in this study we only included the nine TBMs that had hourly GPP estimates at more than 20 sites in order to derive enough γ_A samples for our analysis (Extended Data Fig. 10 and Supplementary Table 3). In addition, we used the boreal ecosystem productivity simulator (BEPS) – one of the nine TBMs in NACP – to test the possibility of incorporating an optimality model (see section 4 of the Methods) in TBMs to improve the simulation of light acclimation. BEPS is a two-leaf enzyme

kinetic model that has been extensively validated against measured carbon and water fluxes over different biomes ^{51,52} and its parameterization and structure is described in detail elsewhere ^{53,54}.

280

281

282

283

284

285

286

287

288

289

290

291

292

293

294

295

296

297

298

299

300

278

279

3. Calculation of the photosynthetic light acclimation rate (γ_A)

Following the derivation of seasonal varying A_{max} from eddy covariance measurements and TBM estimates, we analyzed the relationship between A_{max} and its corresponding \overline{PPFD}_{10} and defined γ_A as the rate of light acclimation of photosynthesis. Since fAPAR and T_{air} also change across the season and might influence the variations of A_{max}, it is necessary to remove the effects of fAPAR and T_{air} on A_{max} to identify the \overline{PPFD}_{10} - A_{max} relationship. To do so, we grouped the A_{max} and \overline{PPFD}_{10} pairs into bins, with each bin confined to a narrow interval of fAPAR and T_{air} . We used an interval of fAPAR of 0.02 and an interval of T_{air} of 1 °C. Then, in each bin, we regressed A_{max} against \overline{PPFD}_{10} to obtain γ_A . The specific intervals of fAPAR and T_{air} were chosen to ensure the number of the pairs of \overline{PPFD}_{10} and A_{max} was large enough for a regression analysis and small enough to assume fAPAR and Tair were nearly constant within each bin. In addition, water stress (i.e. high VPD, low soil water content) may also influence the variations of A_{max} ^{55,56}, so we used a strict threshold to remove the drought-affected data points using the 10day average of the ratio of actual evapotranspiration (ET) to potential ET (α), which has been suggested as an effective indicator of soil moisture stress on photosynthesis 56 . We calculated α using the actual ET measured by eddy covariance and the potential ET calculated from the Priestley-Taylor equation ⁵⁷. We excluded days with $\alpha \le 0.8$ as they were deemed waterstressed. In addition to applying this threshold, we also removed shrubland and savanna sites as they are sensitive to water stress. After the removal, the average VPD for all \overline{PPFD}_{10} -A_{max} pairs was 0.47 ± 0.43 kPa, or 90% of the data pairs had VPD < 1 kPa. We ended up with 26985 pairs

of A_{max} and \overline{PPFD}_{10} in total from 118 sites. The regression of A_{max} and \overline{PPFD}_{10} was carried out for each bin only if there were at least 20 pairs of A_{max} and \overline{PPFD}_{10} in it (900 bins in total; Extended Data Fig. 7) for cross-sites analysis and at least 5 pairs for PFT-specific analysis. Since every site on average only had 229 pairs of A_{max} and \overline{PPFD}_{10} , we were not able to bin these pairs at each site and calculate γ_A for each site specifically. For the derivation of A_{max} and γ_A from TBMs estimated fluxes, we followed the same procedures as used for the flux observations. We also derived A standardized to a PPFD of 2000 μ mol m⁻² s⁻¹ (A_{2000}) from the fitted light response curves (Equation 1) to study light acclimation as the response of A_{2000} to \overline{PPFD}_{10} and presented the results in Extended Data Fig. 2. However, for the convenience of incorporating light acclimation in TBMs and providing a consistent benchmark for future model-data comparisons, we presented the results in the main text using A_{max} .

4. The optimality model for Vc_{max25}

The maximum carboxylation rate (Vc_{max}; µmol m⁻² s⁻¹) is often used to represent the activity of the photosynthetic enzyme Ribulose-1,5-bisphosphate carboxylase/oxygenase (Rubisco) in light saturated leaves, meaning the increase of A_{max} to PPFD is related to an increase of Vc_{max} to PPFD. A recent study developed an optimality model for Vc_{max} ¹⁹ based on the coordination hypothesis ²¹ and the least-cost hypothesis ¹⁷ to estimate leaf Vc_{max} using various climate variables including PPFD. This optimality model therefore provides an approach to include the impact of PPFD on A_{max} in TBMs.

According to the classic Farquhar biochemical model ⁵⁸, the photosynthetic rate, A, is limited by either Vc_{max}, or by the electron transport rate for the regeneration of ribulose-1,5,-bisphosphate (RuBP; J; µmol m⁻² s⁻¹). The two processes are represented by equations (3) and (4), respectively:

324
$$A_c = V c_{max} \frac{c_i - \Gamma^*}{c_i + K}$$
 (3)

325
$$A_j = \left(\frac{J}{4}\right) \frac{C_i - \Gamma^*}{C_i + 2\Gamma^*} \tag{4}$$

- where Ci is the intercellular CO_2 concentration (Pa), Γ^* is the CO_2 compensation point (Pa) in
- 327 the absence of mitochondrial respiration, and K (Pa) is estimated as:

$$328 K = K_c \left(1 + \frac{o_i}{\kappa_o} \right) (5)$$

- where K_c and K_o are Michaelis-Menten coefficients of Rubisco activity for CO₂ and O₂ (Pa), and
- O_i is the intercellular O₂ concentration (Pa). K and Γ^* are temperature dependent variables and
- the calculation of them is introduced in detail by Smith et al. 19. J is dependent on a response
- curve of the incident photosynthetically active photon flux density (I; µmol m⁻² s⁻¹), converging
- at the maximum electron transport rate (J_{max} ; μ mol m⁻² s⁻¹):

334
$$\theta J^2 - (\varphi I + J_{max})J + \varphi IJ_{max} = 0$$
 (6)

- where θ is the curvature of the light response curve and assumed to be 0.85, and φ is the
- maximum quantum yield of photosynthetic electron transport fixed at 0.257 mol mol⁻¹.
- Combining equations (4) and (6) gives:

338
$$A_j = \varphi I \frac{c_i - \Gamma^*}{c_i + 2\Gamma^*} \left(\frac{\varpi^*}{8\theta}\right)$$
 (7)

where ω^* is derived from the following two equations:

340
$$\omega^* = 1 + \omega - \sqrt{(1+\omega)^2 - 4\theta\omega}$$
 (8)

- For the calculation of ϖ , c was assumed to be a constant at 0.053 ¹⁹, and m is $\frac{C_i \Gamma^*}{C_i + 2\Gamma^*}$. According
- 343 to the coordination hypothesis, photosynthesis under typical daytime conditions is close to the

- point where Rubisco-limited and electron transport-limited rate are equal, meaning $A_c = A_j$.
- 345 Therefore, by combining equation (3) and (7), we get:

346
$$Vc_{max} = \varphi I \frac{c_i + K}{c_i + 2\Gamma^*} \left(\frac{\varpi^*}{8\theta} \right)$$
 (10)

- This equation implies that Vc_{max} adjusts to incident light levels over intermediate timescales, as I
- is equivalent to \overline{PPFD} . Following the least-cost hypothesis, C_i is sustained at an optimal level to
- minimize the carbon cost of water use ¹⁷:

350
$$\frac{C_i}{C_a} = \frac{\Gamma^*}{C_a} + \left(1 - \frac{\Gamma^*}{C_a}\right) \frac{\xi}{\xi + \sqrt{VPD}}$$
 (11)

351
$$\xi = \sqrt{\beta \frac{K + \Gamma^*}{1.6\eta^*}}$$
 (12)

- where ξ defines the sensitivity of C_i/C_a to VPD and β is a constant 146. More details about the
- 353 calculation of C_i are introduced in Smith et al. ¹⁹.
- In this study, we used 10-day average climate variables acquired from the meteorological
- measurements of eddy covariance sites, including PPFD, Tair, VPD to drive the optimality model
- 356 to get the 10-day Vc_{max}, normalized Vc_{max} from growing temperature to 25 °C (Vc_{max25}) and then
- 357 linearly interpolated 10-day Vc_{max25} to daily values to drive BEPS.
- Note that the optimality model provides us with Vc_{max} at the growing temperature. We
- normalized Vc_{max} to 25 °C using a modified Arrhenius temperature response function ⁵⁹ used in
- 360 BEPS following equation (13):

361
$$Vc_{max} = Vc_{max25} \exp[H_a(T_l - T_{ref})/(T_{ref}RT_l)] \frac{1 + \exp(\frac{T_{ref}\Delta S - H_d}{T_{ref}R})}{1 + \exp(\frac{T_l\Delta S - H_d}{T_lR})}$$
 (13)

- where T_1 is the growing temperature of leaf in Kelvin, T_{ref} is the reference temperature of Vc_{max25}
- 363 (298.15K), H_a is the activation energy for carboxylation (55000 J mol⁻¹), H_d is the deactivation

energy (200000 J mol⁻¹), ΔS is an entropy term (663.1 J mol⁻¹ K⁻¹) and R is the universal gas 364 constant (8.314 J mol⁻¹ K⁻¹). 365 366 **Data Availability** 367 368 This study used openly available eddy covariance measurements provided by FLUXNET2015 369 Tier 1 dataset (https://fluxnet.fluxdata.org/data/fluxnet2015-dataset/), and the North America 370 Carbon Program site-level interim synthesis data downloaded from https://daac.ornl.gov/NACP/. 371 The MODIS fAPAR time series (MOD15A2H) for eddy covariance sites were acquired from 372 https://lpdaac.usgs.gov/tools/appeears. 373 **Code Availability** 374 375 The code to derive maximum ecosystem photosynthetic rate from eddy covariance 376 measurements is available at https://github.com/bgctw/REddyProc; the code of the optimality model for Vc_{max} is available at https://github.com/SmithEcophysLab/optimal_vcmax_R; the 377 378 code of the Boreal Ecosystem Productivity Simulator is available at https://github.com/JChen-379 UToronto/BEPS hourly site 4.02. 380 381 382 **Acknowledgements** 383 X.L. and T.F.K. were supported by the NASA Terrestrial Ecology Program IDS Award 384 NNH17AE86I. T.F.K. also acknowledges support by the Director, Office of Science, Office of 385 Biological and Environmental Research of the US Department of Energy under Contract DE-386 AC02-05CH11231 as part of the RuBiSCo SFA. This work used eddy covariance data acquired

387	and shared by the FLUXNET community, including these networks: AmeriFlux, AfriFlux,
388	AsiaFlux, CarboAfrica, CarboEuropeIP, CarboItaly, CarboMont, ChinaFlux, Fluxnet-Canada,
389	GreenGrass, ICOS, KoFlux, LBA, NECC, OzFlux-TERN, TCOS-Siberia, and USCCC. The
390	ERA-Interim reanalysis data are provided by ECMWF and processed by LSCE. The FLUXNET
391	eddy covariance data processing and harmonization was carried out by the European Fluxes
392	Database Cluster, AmeriFlux Management Project, and Fluxdata project of FLUXNET, with the
393	support of CDIAC and ICOS Ecosystem Thematic Center, and the OzFlux, ChinaFlux and
394	AsiaFlux offices. The eddy covariance site used is listed in Table S2. We thank the North
395	American Carbon Program (NACP) for making their site-level synthesis and modelling data
396	publicly available. The terrestrial biosphere models and the eddy covariance sites participating in
397	NACP are acknowledged in Table S3 and S4.
398	Author contributions : X.L. and T.F.K. designed the study; X.L. performed the analysis and led
399	the writing; T.F.K. contributed to the writing.
400	The authors declare no conflict of interest.

402 Reference:

401

- IPCC. Climate Change 2013: The Physical Science Basis. Contribution of Working Group
 I to the Fifth Assessment Report of the Intergovernmental Panel on Climate Change.
 Cambridge University Press: Cambridge, United Kingdom and New York, NY, USA,
 2013 doi:doi:10.1017/CBO9781107415324.
- 407 2 Campbell GS, Norman JM. *An Introduction to Environmental Biophysics*. Springer Science & Business Media, 2012.
- Lambers H, Chapin FS, Pons TL. Photosynthesis. In: *Plant Physiological Ecology*.
 Springer New York: New York, NY, 2008, pp 11–99.
- 411 4 Ögren E, Evans JR. Photosynthetic light-response curves. *Planta* 1993; **189**: 182–190.
- Fisher JB, Huntzinger DN, Schwalm CR, Sitch S. Modeling the Terrestrial Biosphere. *Annu Rev Environ Resour* 2014; **39**: 91–123.
- Walters MB, Field CB. Photosynthetic light acclimation in two rainforest Piper species

- with different ecological amplitudes. *Oecologia* 1987; **72**: 449–456.
- Walters RG, Horton P. Acclimation of Arabidopsis thaliana to the light environment: Changes in composition of the photosynthetic apparatus. *Planta* 1994; **195**: 248–256.
- 418 8 Bailey S, Walters RG, Jansson S, Horton P. Acclimation of Arabidopsis thaliana to the
- Bailey S, Walters RG, Jansson S, Horton P. Acclimation of Arabidopsis thaliana to the light environment: The existence of separate low light and high light responses. *Planta* 2001; **213**: 794–801.
- Sims DA, Pearcy RW. Photosynthetic characteristics of a tropical forest understory herb, Alocasia macrorrhiza, and a related crop species, Colocasia esculenta grown in contrasting light environments. *Oecologia* 1989; **79**: 53–59.
- Poorter H, Niinemets Ü, Ntagkas N, Siebenkäs A, Mäenpää M, Matsubara S *et al.* A meta-analysis of plant responses to light intensity for 70 traits ranging from molecules to whole plant performance. *New Phytol* 2019. doi:10.1111/nph.15754.
- Hikosaka K, Terashima I. A model of the acclimation of photosynthesis in the leaves of C3 plants to sun and shade with respect to nitrogen use. *Plant, Cell Environ* 1995; **18**: 605–618.
- Warren CR, Adams MA. Distribution of N, Rubisco and photosynthesis in Pinus pinaster and acclimation to light. *Plant, Cell Environ* 2001; **24**: 597–609.
- 432 13 Laisk A, Nedbal L, Govindjee. *Photosynthesis in silico*. Springer Netherlands: Dordrecht, 2009 doi:10.1007/978-1-4020-9237-4.
- Baldocchi D. 'Breathing' of the terrestrial biosphere: lessons learned from a global network of carbon dioxide flux measurement systems. *Aust J Bot* 2008; **56**: 1.
- Baldocchi DD. How eddy covariance flux measurements have contributed to our understanding of Global Change Biology. *Glob Chang Biol* 2020; **26**: 242–260.
- 438 16 Keenan TF, Migliavacca M, Papale D, Baldocchi D, Reichstein M, Torn M *et al.*439 Widespread inhibition of daytime ecosystem respiration. *Nat Ecol Evol* 2019; **3**.
 440 doi:10.1038/s41559-019-0809-2.
- Prentice IC, Dong N, Gleason SM, Maire V, Wright IJ. Balancing the costs of carbon gain and water transport: Testing a new theoretical framework for plant functional ecology. *Ecol Lett* 2014; 17: 82–91.
- Wang H, Prentice IC, Keenan TF, Davis TW, Wright IJ, Cornwell WK *et al.* Towards a universal model for carbon dioxide uptake by plants. *Nat Plants* 2017; **3**: 734–741.
- Smith NG, Keenan TF, Colin Prentice I, Wang H, Wright IJ, Niinemets Ü *et al.* Global photosynthetic capacity is optimized to the environment. *Ecol Lett* 2019; **22**: 506–517.
- Keenan TF, Prentice IC, Canadell JG, Williams CA, Wang H, Raupach M *et al.* Recent pause in the growth rate of atmospheric CO2 due to enhanced terrestrial carbon uptake.
 Nat Commun 2016; 7: 13428.
- 451 21 Maire V, Martre P, Kattge J, Gastal F, Esser G, Fontaine S *et al.* The Coordination of Leaf Photosynthesis Links C and N Fluxes in C3 Plant Species. *PLoS One* 2012; 7: e38345.
- Bauerle WL, Oren R, Way DA, Qian SS, Stoy PC, Thornton PE *et al.* Photoperiodic regulation of the seasonal pattern of photosynthetic capacity and the implications for carbon cycling. *Proc Natl Acad Sci U S A* 2012; **109**: 8612–8617.
- He L, Chen JM, Gonsamo A, Luo X, Wang R, Liu Y *et al.* Changes in the Shadow: The Shifting Role of Shaded Leaves in Global Carbon and Water Cycles Under Climate Change. *Geophys Res Lett* 2018; **45**: 5052–5061.
- Ogren E, Rosenqvist E. On the significance of photoinhibition of photosynthesis in the field and its generality among species. *Photosynth Res* 1992; **33**: 63–71.

- Greer DH, Berry JA. Planta role of light and temperature, and requirement. 1986; : 253–260.
- Öquist G, Chow WS, Anderson JM. Photoinhibition of photosynthesis represents a
 mechanism for the long-term regulation of photosystem II. *Planta* 1992; **186**: 450–460.
- Daniel E. The temperature dependence of photoinhibition in leaves of Phaseolus vulgaris (L.) influence of CO2 and O2 concentrations. *Plant Sci* 1997; **124**: 1–8.
- 467 28 Tyystjärvi E. *Photoinhibition of Photosystem II**. 2013 doi:10.1016/B978-0-12-405210-468 9.00007-2.
- Katul GG, Palmroth S, Oren R. Leaf stomatal responses to vapour pressure deficit under current and CO2-enriched atmosphere explained by the economics of gas exchange. *Plant, Cell Environ* 2009; **32**: 968–979.
- 472 30 Oren R, Sperry JS, Katul GG, Pataki DE, Ewers BE, Phillips N *et al.* Survey and synthesis of intra- and interspecific variation in stomatal sensitivity to vapour pressure deficit. *Plant Cell Environ* 1999; **22**: 1515–1526.
- Laing WA. Temperature and light response curves for photosynthesis in kiwifruit (Actinidia chinensis) cv. Hayward. *New Zeal J Agric Res* 1985; **28**: 117–124.
- Leverenz JW. The effects of illumination sequence, CO2 concentration, temperature and acclimation on the convexity of the photosynthetic light response curve. *Physiol Plant* 1988; **74**: 332–341.
- Bazzaz FA, Carlson RW. Photosynthetic acclimation to variability in the light environment of early and late successional plants. *Oecologia* 1982; **54**: 313–316.
- Valladares F, Martinez-Ferri E, Balaguer L, Perez-Corona E, Manrique E. Low leaf-level response to light and nutrients in Mediterranean evergreen oaks: A conservative resource-use strategy? *New Phytol* 2000; **148**: 79–91.
- Poorter H, Evans JR. Photosynthetic nitrogen-use efficiency of species that differ inherently in specific leaf area. *Oecologia* 1998; **116**: 26–37.
- Kattge J, Knorr W, Raddatz T, Wirth C. Quantifying photosynthetic capacity and its relationship to leaf nitrogen content for global-scale terrestrial biosphere models. *Glob Chang Biol* 2009; **15**: 976–991.
- 490 37 Murchie EH, Horton P. Acclimation of photosynthesis to irradiance and spectral quality in 491 British plant species: Chlorophyll content, photosynthetic capacity and habitat preference. 492 *Plant, Cell Environ* 1997; **20**: 438–448.
- 493 38 Alter P, Dreissen A, Luo FL, Matsubara S. Acclimatory responses of Arabidopsis to 494 fluctuating light environment: Comparison of different sunfleck regimes and accessions. 495 *Photosynth Res* 2012; **113**: 221–237.
- Slattery RA, Walker BJ, Weber APM, Ort DR. The impacts of fluctuating light on crop performance. *Plant Physiol* 2018; **176**: 990–1003.
- 498 40 Murchie EH, Hubbart S, Chen Y, Peng S, Horton P. Acclimation of rice photosynthesis to irradiance under field conditions. *Plant Physiol* 2002; **130**: 1999–2010.
- Thornton PE, Zimmermann NE. An improved canopy integration scheme for a Land Surface Model with prognostic canopy structure. *J Clim* 2007; **20**: 3902–3923.
- Grant RF, Barr AG, Black TA, Margolis HA, Dunn AL, Metsaranta J *et al.* Interannual variation in net ecosystem productivity of Canadian forests as affected by regional weather patterns A Fluxnet-Canada synthesis. *Agric For Meteorol* 2009; **149**: 2022–2039.
- 806 43 Ryu Y, Baldocchi DD, Kobayashi H, Van Ingen C, Li J, Black TA et al. Integration of

- MODIS land and atmosphere products with a coupled-process model to estimate gross primary productivity and evapotranspiration from 1 km to global scales. *Global Biogeochem Cycles* 2011; **25**: GB4017.
- 510 44 Chen JM, Ju W, Ciais P, Viovy N, Liu R, Liu Y *et al.* Vegetation structural change since 1981 significantly enhanced the terrestrial carbon sink. *Nat Commun* 2019; **10**: 4–10.
- Luo X, Croft H, Chen JM, He L, Keenan TF. Improved estimates of global terrestrial photosynthesis using information on leaf chlorophyll content. *Glob Chang Biol* 2019; : 1–16.
- Pastorello GZ, Papale D, Chu H, Trotta C, Agarwal DA, Canfora E *et al.* A new data set to keep a sharper eye on land-air exchanges. *Eos (Washington DC)* 2017; **98**. doi:https://doi.org/10.1029/2017EO071597.
- Lasslop G, Reichstein M, Papale D, Richardson A, Arneth A, Barr A *et al.* Separation of net ecosystem exchange into assimilation and respiration using a light response curve approach: Critical issues and global evaluation. *Glob Chang Biol* 2010; **16**: 187–208.
- 521 48 Schaefer K, Schwalm CR, Williams C, Arain MA, Barr A, Chen JM *et al.* A model-data comparison of gross primary productivity: Results from the north American carbon program site synthesis. *J Geophys Res Biogeosciences* 2012; **117**: 1–15.
- 524 49 Ricciuto DM, Schaefer K, Thornton PE, Cook RB, Anderson R, Arain MA *et al.* NACP 525 Site: Terrestrial Biosphere Model Output Data in Original Format. 2013. 526 doi:10.3334/ornldaac/1192.
- 527 50 Ricciuto DM, Schaefer K, Thornton PE, Davis K, Cook RB, Liu S *et al.* NACP Site: Terrestrial Biosphere Model and Aggregated Flux Data in Standard Format. 2013. doi:10.3334/ornldaac/1183.
- 530 51 Gonsamo A, Chen JM, Price DT, Kurz W a., Liu J, Boisvenue C et al. Improved
 531 assessment of gross and net primary productivity of Canada's landmass. J Geophys Res
 532 Biogeosciences 2013; 118: 1546–1560.
- Wang Q, Tenhunen J, Falge E, Bernhofer C, Granier A, Vesala T. Simulation and scaling of temporal variation in gross primary production for coniferous and deciduous temperate forests. *Glob Chang Biol* 2004; **10**: 37–51.
- 536 Chen J., Liu J, Cihlar J, Goulden M. Daily canopy photosynthesis model through temporal and spatial scaling for remote sensing applications. *Ecol Modell* 1999; **124**: 99–119.
- 538 54 Luo X, Chen JM, Liu J, Black TA, Croft H, Staebler R *et al.* Comparison of Big-Leaf,
 539 Two-Big-Leaf, and Two-Leaf Upscaling Schemes for Evapotranspiration Estimation
 540 Using Coupled Carbon-Water Modeling. *J Geophys Res Biogeosciences* 2018; 123: 207–
 541 225.
- 542 Su L, Baldocchi DD. Seasonal trends in photosynthetic parameters and stomatal 543 conductance of blue oak (Quercus douglasii) under prolonged summer drought and high 544 temperature. *Tree Physiol* 2003; **23**: 865–877.
- 545 56 Stocker BD, Zscheischler J, Keenan TF, Prentice IC, Peñuelas J, Seneviratne SI.
 546 Quantifying soil moisture impacts on light use efficiency across biomes. *New Phytol* 2018.
 547 doi:10.1111/nph.15123.
- 548 57 Fisher JB, Whittaker RJ, Malhi Y. ET come home: Potential evapotranspiration in geographical ecology. *Glob Ecol Biogeogr* 2011; **20**: 1–18.
- Farquhar GD, von Caemmerer S, Berry JA. A biochemical model of photosynthetic CO2 assimilation in leaves of C 3 species. *Planta* 1980; **149**: 78–90.
- 552 59 Medlyn BE, Dreyer E, Ellsworth D, Forstreuter M, Harley PC, Kirschbaum MUF et al.

Temperature response of parameters of a biochemically based model of photosynthesis. II. A review of experimental data. *Plant, Cell Environ* 2002; **25**: 1167–1179.

Fig. 1 | The relationships between the maximum photosynthetic rate (A_{max}) of ecosystems and 10-day average PPFD (\overline{PPFD}_{10}). (a) the rate of photosynthetic light acclimation (γ_A ; mol mol⁻¹; μ mol C m⁻² s⁻¹ per μ mol photon m⁻² s⁻¹) under different vegetation densities (indicated by fraction of absorbed PAR; fAPAR) and daytime air temperature (T_{air}), and the black dots indicate where there is a significant (p < 0.1) linear correlation between \overline{PPFD}_{10} and A_{max} . A_{max} and \overline{PPFD}_{10} pairs are grouped by fAPAR and T_{air} , where the interval of fAPAR is 0.02 and the interval of T_{air} is 1 °C. Only bins with at least 20 pairs of A_{max} and \overline{PPFD}_{10} are plotted. (b) several exemplary and significant (p < 0.05) responses of A_{max} to \overline{PPFD}_{10} under different fAPAR and T_{air} . The shadings indicate 95% confidence interval of the linear regressions. (c) The comparison between ecosystem γ_A derived from flux data and published leaf-level γ_A . For each box, the cross indicates the mean, the center line indicates the median, the box indicates the upper and lower quartiles and the whiskers indicate the 5th and 95th percentiles of the data.

Fig. 2 | Ecosystem photosynthetic light acclimation rate (γ_A) changes with (a) vegetation densities (fAPAR), (b) daytime temperature (T_{air}), (c) plant functional types (PFTs) and (d) vapor pressure deficit (VPD). The shadings in (a) and (b) indicate one standard deviation of γ_A (n > 5; n is the number of bins with significant γ_A (p < 0.1)) for each fAPAR and T_{air} , the red lines indicate the detectability of photosynthetic light acclimation (i.e. n divided by the total number of bins). (c) γ_A of each PFT. For each box, the cross indicates the mean, the center line indicates the median, the box indicates the upper and lower quartiles and the whiskers indicate

the 5th and 95th percentiles of the data. The acronyms of PFTs in (c) stand for croplands (CRO), deciduous broadleaf forests (DBF), evergreen broadleaf forests (EBF), evergreen needleleaf forests (ENF), mixed forests (MF) and grasslands (GRA). '*' indicates that γ_A of CRO is statistically different than γ_A of other PFTs (*t*-test, p < 0.05); (d) The impact of VPD on γ_A . The significance level of light acclimation and the sign of γ_A change with VPD. For each box, the point indicates the mean, the box indicates the upper and lower quartiles and the whiskers indicate the 5th and 95th percentiles of the data. Red indicates bins with $\gamma_A > 0$ and blue box indicates bins with $\gamma_A < 0$.

Fig. 3 | Incorporating photosynthetic light acclimation into terrestrial biosphere models. (a) The distribution of γ_A derived from eddy-covariance measurements (black) and from the GPP estimates of 9 terrestrial biosphere models (TBMs; other colors) participating in the North American Carbon Program. (b) Incorporating the optimality model into a TBM (the boreal ecosystem productivity simulator (BEPS)) to improve the estimation of photosynthetic light acclimation. The distribution of eddy covariance-based γ_A is in black, the distribution of γ_A derived from BEPS estimates is in blue and the distribution of γ_A derived from BEPS improved by the optimality model (BEPS-opt) is in red. (c) The intra-annual variation and (d) inter-annual variation of estimated and "measured" gross primary productivity (GPP). BEPS and BEPS-opt stand for the GPP estimated by the two models; GPP-DT stands for "measured" GPP derived from net carbon fluxes using the day-time partition method. For each box, the cross indicates the mean, the center line indicates the median, the box indicates the lower and upper quartiles and

- the whiskers indicate the 5th and 95th percentiles of the data. '*' indicates that BEPS-opt is
- significantly improved (t-test, p < 0.05) compared to BEPS.

